Rapid and Accurate Determination of Stern–Volmer Quenching Constants

JOHN V. GOODPASTER and VICTORIA L. McGUFFIN*

Department of Chemistry, Michigan State University, East Lansing, Michigan 48824-1322

In this work, a novel system has been designed, characterized, and validated for the determination of fluorescence quenching constants. Capillary flow injection methods are used to automate the preparation and mixing of the fluorophore and quencher solutions. Because of the small diameter of the capillary (75–200 μm), fluorescence measurements can be made without corrections for primary and secondary absorbance effects. The fluorescence spectrometer is equipped with a charge-coupled device (CCD) that has a detection limit of 3.0×10^{-9} M (2.3 ppb) and a linear dynamic range of 10^5 for integration times of 0.01–10 s. This spectrometer has a 300 nm spectral range with 1 nm resolution, allowing the fluorescence quenching constants to be calculated at single wavelengths or over integrated wavelength ranges. This system was validated by comparison to traditional methods for the determination of Stern–Volmer constants for alternant and nonalternant polycyclic aromatic hydrocarbons with nitromethane and triethylamine.

Index Headings: **Fluorescence; Fluorescence quenching; Instrumentation; Polycyclic aromatic hydrocarbons.**

INTRODUCTION

Quenching is usually considered to be a detrimental phenomenon in fluorescence spectroscopy. However, the deliberate quenching of fluorescence can be used to analytical advantage if applied in a judicious and carefully controlled manner. This method can provide valuable photophysical and photochemical information about an individual fluorophore that can be used for its classification or identification. In addition, when combined with a separation method, it can be used to simplify the qualitative and quantitative analysis of complex samples by selective discrimination against interfering components.

Fluorescence quenching can be defined as any process that decreases the observed fluorescence power from a sample.[1] These processes include trivial phenomena such as primary and secondary absorption as well as light scattering due to changes in the refractive index or turbidity of a solution. Of more use in analytical applications is dynamic quenching, which involves the collision and subsequent formation of a transient complex between an excited-state fluorophore and a ground-state quencher.[2,3] Because this complex must be formed during the excited-state lifetime of the fluorophore, dynamic or collisional quenching is diffusion controlled. The excited-state complex dissociates upon radiative or nonradiative deactivation, leaving both the fluorophore and quencher in the ground state. This form of quenching is described by the Stern–Volmer equation.[2,3]

$$\Phi_f^\circ/\Phi_f \approx P_f^\circ/P_f = 1 + k_d\tau_f^\circ C_q = 1 + K_d C_q \qquad (1)$$

where Φ_f° and Φ_f are the quantum efficiencies of the fluorophore in the absence and presence of the quencher, respectively. These quantum efficiencies are directly proportional to the measured fluorescence powers (P_f° and P_f, respectively) provided that the source power, efficiency of optical irradiation and collection, and fluorophore absorbance remain constant. Finally, τ_f° is the fluorescence lifetime of the unquenched fluorophore, C_q is the molar concentration of the quencher, k_d is the bimolecular rate constant for dynamic quenching, and K_d is the Stern–Volmer constant.

In static quenching, a complex is formed between a ground-state fluorophore and a ground-state quencher.[2,3] This ground-state complex is stable with spectral properties that will necessarily differ from those of the uncomplexed fluorophore. For static quenching, a linear relationship is observed between the quantum efficiency or fluorescence power ratio and the quencher concentration:[2,3]

$$\Phi_f^\circ/\Phi_f \approx P_f^\circ/P_f = 1 + K_s C_q \qquad (2)$$

where K_s is the equilibrium formation constant of the fluorophore–quencher complex, and all other variables are as defined previously.

When only a single quenching mechanism is present, a Stern–Volmer plot of (P_f°/P_f) vs. C_q should yield a straight line with a slope equal to the quenching constant and an intercept of unity. However, if the quencher absorbs at the excitation or emission wavelength, there will be a positive deviation from linearity in the Stern–Volmer plot. This absorbance effect can be corrected through a modified form of the Stern–Volmer equation:[4,5]

$$(P_f^\circ/P_f)\{[1 - \exp(-2.3\epsilon_{q,ex}bC_q)]/2.3\epsilon_{q,ex}bC_q\} \times \{[1 - \exp(-2.3\epsilon_{q,em}bC_q)]/2.3\epsilon_{q,em}C_q\} = 1 + K_d C_q \qquad (3)$$

where $\epsilon_{q,ex}$ and $\epsilon_{q,em}$ are the molar absorptivity of the quencher at the excitation and emission wavelengths, respectively; b is the pathlength of the cell; and C_q is the concentration of the quencher.

An alternative method that is not affected by static quenching or by absorbance effects relies on the fact that dynamic quenching is a nonradiative process that decreases the observed fluorescence lifetime. Hence, the attenuation of lifetime as a function of quencher concentration can also be used to determine quenching constants. In this approach, the ratio of unquenched to quenched fluorescence lifetime (τ_f°/τ_f) is calculated as a function of the quencher concentration (C_q). This approach can quantify the amount of dynamic quenching directly, even in the presence of absorbance effects or ground-state complexation.[6,7]

To date, the development of quenching as a tool for

Received 11 January 1999; accepted 10 March 1999.

* Author to whom correspondence should be sent.

0003-7028/99/5308-1000$2.00/0

chemical analysis has been relatively limited. This situation is largely due to the methods for determining Stern–Volmer constants, which remain both time and labor intensive. In a typical study, a series of solutions with constant fluorophore concentration and varying quencher concentration is prepared, and the attenuation of the fluorescence power (or lifetime) at a single wavelength is measured. While this technique is effective, it is also slow, tedious, and prone to experimental error. Hence, such an approach is not well suited for the evaluation of large numbers of fluorophores and quenchers.

Recently, some novel approaches to quenching experiments have been proposed. For example, Desilets et al. used a gradient pump from a liquid chromatograph to linearly increase the concentration of quencher in a flowing stream of a fluorophore, measuring the decrease in fluorescence power at a single wavelength.[8] This method required little solution preparation, allowed for greater precision in solution concentrations, acquired a large number of fluorescence power ratios in each quenching experiment, and increased the overall speed of the quenching measurements. However, this method was limited to the analysis of one fluorophore–quencher pair at a single wavelength, and acquired only one fluorescence power ratio at each quencher concentration. Moreover, it was reliant on the precision of the linear gradient program to calculate the quencher concentration and did not make corrections for absorbance effects.

A different approach was taken by Chen et al., who measured quenching constants by using a laser for excitation in a capillary flow cell.[4] The short pathlength of the capillary minimized absorption by the quencher at both the excitation and emission wavelengths. However, this system required premixed solutions of the fluorophore and quencher and was also limited to a single wavelength. A final approach for determining the quenching constants of a number of fluorophores involved separating a complex mixture by using capillary liquid chromatography with laser-induced fluorescence detection.[4,5] The observed peak heights both with and without quencher dissolved in the mobile phase were used to calculate conditional quenching constants at the detected wavelength. While this approach obviated the need for purifying the fluorophores as well as allowed for the analysis of complex samples, it required the use of lengthy chromatographic separations. Furthermore, it was limited to a single wavelength for all fluorophores, and only one fluorescence power ratio was used to calculate each quenching constant.[4,5]

In the present study, novel instrumentation for evaluating Stern–Volmer constants has been developed that combines the advances of previous studies while overcoming many of their limitations. In this system, solution preparation is automated through the use of flow injection techniques. This approach allows the measurement of quenching constants for many fluorophores in a single experiment with precise control over the quencher concentration. Moreover, a large number of replicate measurements can be made at each quencher concentration, leading to greater accuracy and precision. A capillary flow cell is used to eliminate absorbance effects, and a charge-coupled device (CCD) detector allows for the calculation of Stern–Volmer constants on the basis of either single wavelengths or integrated emission spectra. The performance of this system is evaluated and the accuracy and precision are compared with traditional methods for the determination of Stern–Volmer constants.

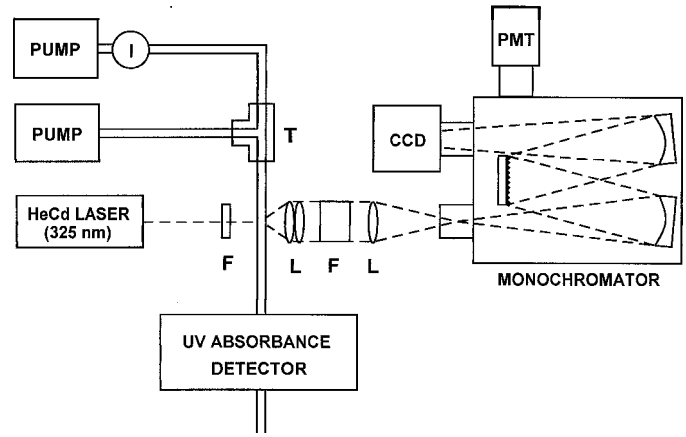

FIG. 1. Schematic diagram of the instrumentation for fluorescence quenching studies. **I**, injection valve; **T**, mixing tee; **F**, filter; **L**, lens; **CCD**, charge-coupled device; **PMT**, photomultiplier tube.

EXPERIMENTAL

Reagents. Quinine sulfate (Baker) is used as received. Stock solutions of quinine sulfate are prepared in 0.05 M H_2SO_4 in deionized, distilled water (Corning Glass Works, Model MP-3A). Pyrene (MCB), fluoranthene (Aldrich), benzo(*a*)pyrene (Aldrich), and benzo(*b*)fluoranthene (Aldrich) are purified by vacuum sublimation. Reagent-grade nitromethane (EM Science) and triethylamine (Spectrum) are used as received. Stock solutions of the polycyclic aromatic hydrocarbons and quenchers are prepared in high-purity, spectroscopic-grade methanol (Baxter Healthcare, Burdick and Jackson Division).

Flow Injection System. In order to allow for the rapid evaluation of quenching constants, a flow injection apparatus that combines solutions of fluorophores and quenchers has been developed (Fig. 1). The apparatus consists of a dual syringe pump (Brownlee Labs, Model G) that is programmed to deliver a step gradient of the quencher in a suitable solvent at a flow rate of 35 μL/min. A second syringe pump (Applied Biosystems, Model 140) delivers the solvent at 35 μL/min to an injector with a 75 μL loop (Valco Instruments, Model EC6W), which is used to introduce discrete zones of the fluorophore. The solutions of the quencher and fluorophore are combined with a mixing tee (Upchurch Scientific, Model P-727) in fused-silica capillary tubing (200 μm i.d., 375 μm o.d., Polymicro Technologies). After mixing, the fluorophore–quencher solution is directed to a fluorescence detector (*vide infra*) followed by a UV-visible absorbance detector (Jasco, Model UVIDEC-100-V).

Fluorescence System. A ray tracing program (Stellar Software, BEAM4 Optical Ray Tracer) has been used to aid in the design and optimization of the spectroscopic system. In this system, a helium–cadmium laser (Melles Griot, Model 3074-40M, 325 nm, 40 mW) is utilized as the excitation source, and all optics are enclosed within an aluminum housing to minimize light leaks and other

sources of stray light. The flow cell is constructed of fused-silica capillary tubing (75–200 μm i.d., 375 μm o.d., Polymicro Technologies). Fluorescence emission is collected and collimated by using either two $f/2$ fused-silica lenses (Melles Griot, Model 01 LQP 001/066) or a single $f/1$ concave mirror (Oriel, Model 44351). Scattered light originating from the laser is attenuated by passing the collimated emission through either a long-pass glass filter (Andover Corporation, Model ANDV4922) or a liquid filter consisting of an aqueous solution of 2 M KNO_3 contained in a 1 cm cylindrical fused-silica cell (Perfector Scientific). The filtered emission is refocused with an $f/6$ fused-silica lens (Melles Griot, Model 01 LQP 013/066) onto the entrance slit of a 0.34 m Czerny–Turner monochromator (Instruments SA, Model 340E, 300 grooves/mm grating), which is equipped with a photomultiplier tube (PMT) (Hamamatsu, Model R-106) and a charge-coupled device detector [Instruments SA, Model (A)TECCD-2000×800-7]. The CCD detector is thermoelectrically cooled and is maintained at a temperature of −40 °C. Instrument control and data acquisition are provided by commercially available electronic interfaces (Instruments SA, Model DS1010 and Model CCD 2000) and the associated software (Instruments SA, Spectramax for Windows, Version 2.76).

For purposes of validation and performance evaluation, the system described above is compared with a commercially available scanning fluorimeter (Hitachi, Model F-4500) with a 1 cm cuvette cell. This fluorimeter contains a 150 W xenon lamp, excitation and emission monochromators (900 grooves/mm grating, 2.5 nm bandpass), and a PMT detector, which is operated at 700 V.

Calculations. For the characterization studies, the fluorescence spectra of quinine sulfate are integrated from 370 to 540 nm, and the integrated power is plotted vs. the variable of interest. For calculations of the signal-to-noise (S/N) ratio, the signal is defined as the height of the quinine sulfate emission spectrum at its wavelength of maximum intensity (450 nm). The noise is calculated by first smoothing the spectrum by using a Savitsky–Golay routine[9] with a second-order polynomial and 213/n points, where n is the number of pixels that are horizontally binned on the CCD chip. The smoothed spectrum is then subtracted from the original spectrum and the standard deviation of the remaining noise from 445 to 455 nm is calculated. The logarithm of the calculated S/N ratio is then plotted vs. the logarithm of the signal.

Stern–Volmer plots are prepared by calculating the fluorescence power at a single wavelength or an integrated range of wavelengths as a function of the quencher concentration. The wavelength range for each fluorophore is as follows: pyrene (350–500 nm), fluoranthene (380–560 nm), benzo(*a*)pyrene (370–510 nm), and benzo(*b*)fluoranthene (373–560 nm). The ratio of the fluorescence power in the absence and presence of quencher is then graphed as a function of the quencher concentration. The slope of this graph is determined by linear regression in order to obtain the Stern–Volmer constant according to Eq. 1.

RESULTS AND DISCUSSION

Fluorescence System Characterization. Ray tracing simulations have been used to evaluate the performance of various configurations of the optical components. These studies have identified a number of factors as important to our optical design. For example, simulations demonstrate that a properly oriented plano-convex lens yields higher throughput than a biconvex lens. Moreover, two $f/2$ objective lenses in series provide sharper focus than a single $f/1$ collimating lens. Finally, a concave condenser mirror decreases spherical and chromatic aberrations as well as increases the overall throughput relative to the lens systems.

These simulation results provided the impetus for experimental studies of the optical components and how they affect the system performance. Figures 2A and 2B show the contrasting performance of four different configurations of the collection optics by using a 3.0×10^{-7} M solution of quinine sulfate as a means of comparison. These data indicate that using a concave mirror as the condensing objective with a glass filter to remove laser scatter results in the poorest performance. Although overall throughput is high, as predicted by the ray tracing simulations, the resulting S/N ratio is lower than that for the other optical configurations. In addition, the longest attainable integration time is lower than that for the other configurations. This integration time is ultimately limited by the dark charge from the CCD as well as by background from laser scatter and other stray light, which is highest for this optical configuration. Using two plano-convex lenses as the condensing objective with a glass filter yields similar throughput but higher S/N ratio. Performance is further enhanced by replacing the glass filter with a liquid filter composed of aqueous 2 M KNO_3. When this filter is used, the S/N ratio is higher than that for other optical configurations for any given signal level, and the longest attainable integration time is increased as a result of the lower background. However, because of the smaller aperture of the liquid filter, longer integration times are necessary to achieve the same signal levels as the glass filter. Finally, it has been reported[10] that scattered laser light can be effectively reduced by immersing the fused-silica capillary cell in a refractive-index matching fluid, such as carbon tetrachloride. In the present study, however, there is no significant improvement in S/N ratio because of the larger fluorescence background originating from the cell and fluid.

With the best optical configuration determined from these studies, additional methods of S/N enhancement have been explored such as varying the laser power, entrance slit width, electronic binning of the CCD pixels, and integration time. In the first study, the power of the HeCd laser has been varied from 0.40 to 35 mW. The fluorescence of a standard solution of quinine sulfate increases linearly with laser power, where the square of the correlation coefficient (r^2) is 0.999 and the number of measurements (n) is 11. A logarithmic graph of the S/N ratio vs. signal is linear ($r^2 = 0.982$, $n = 11$) with a slope (m) of 0.54 ± 0.02. Next, the entrance slit width of the monochromator has been varied from 100 to 1000 μm, corresponding to a spectral bandpass of 1–10 nm. The fluorescence of quinine sulfate increases linearly with slit width ($r^2 = 0.997$, $n = 6$), and the logarithmic graph of the S/N ratio vs. signal is also linear ($m = 0.42 \pm 0.05$, $r^2 = 0.937$, $n = 6$). Next, the CCD pixels have been horizontally binned in groups ranging from 1 to 10, cor-

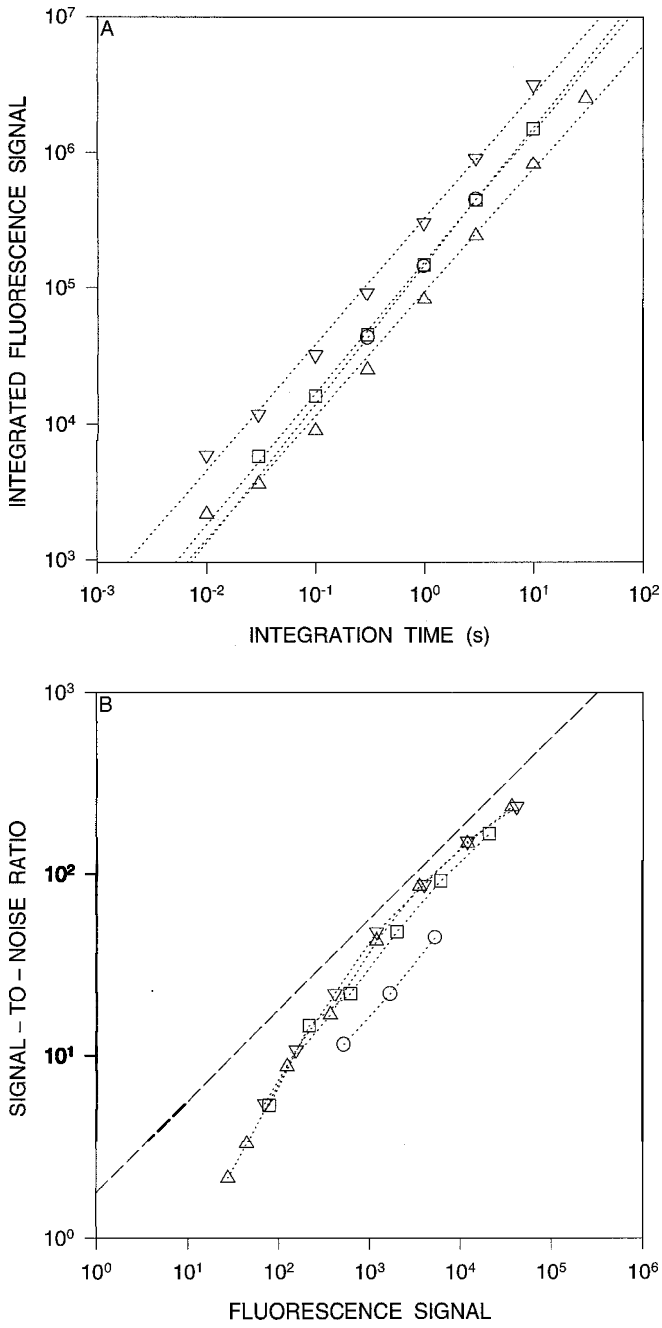

FIG. 2. Effect of optical configuration on the signal (**A**) and S/N ratio (**B**) of a 3.0×10^{-7} M solution of quinine sulfate at various integration times. Data correspond to the following optical configurations: concave mirror, glass filter, and capillary cell (○); two plano-convex lenses, glass filter, and capillary cell (□); two plano-convex lenses, liquid filter, and capillary cell (△); and two plano-convex lenses, liquid filter, and capillary cell contained in refractive-index matching fluid (▽). The dashed line in **B** represents shot-noise-limited conditions with slope (m) of 0.5. Experimental conditions: HeCd laser at 325 nm and 40 mW, 75 μm capillary cell, 0.34 m monochromator with 300 grooves/mm grating and 1 nm bandpass, CCD detector thermoelectrically cooled at −40 °C.

responding to a spectral bandpass of 0.15–1.5 nm. The fluorescence of quinine sulfate increases linearly with the extent of binning ($r^2 = 1.000$, $n = 6$), and the logarithmic graph of the S/N ratio vs. signal is also linear ($m = 0.60 \pm 0.07$, $r^2 = 0.948$, $n = 6$). Finally, the integration time has been varied from 0.01 to 30 s. The fluorescence of quinine sulfate increases linearly with integration time ($r^2 = 1.000$, $n = 6$), and the logarithmic graph of the S/N ratio vs. signal is also linear ($m = 0.59 \pm 0.03$, $r^2 = 0.988$, $n = 6$). For each of these variables, the slope of the logarithmic graphs indicates that the noise is proportional to the square root of the fluorescence signal. This behavior is characteristic of the quantized nature of fluorescence emission, and implies that the spectroscopic system is quantum or shot noise limited.[11–13] Although any of these variables can be used to enhance the S/N ratio in a similar manner, they may have other detrimental effects on the system performance. For example, an increase in these variables will increase the background, thereby decreasing the available dynamic range of the analog-to-digital (A/D) converter and the resulting linear range of the fluorescence measurements and Stern–Volmer plots. Furthermore, an increase in either the slit width or the extent of binning will decrease the spectral resolution, and an increase in laser power may cause photochemical reaction or degradation.[14] The most simple and least detrimental approach to increase the S/N ratio is by means of the integration time, although problems can arise at long integration times (*vide infra*).

The performance of the fluorescence spectrometer has been characterized by means of the calibration curves for quinine sulfate shown in Fig. 3A. Overall, the linearity of the calibration curves is quite good ($r^2 = 0.994-1.000$, $n = 3–6$). Deviations from linearity near the limit of detection arise from blank noise in the signal, which contributes a larger proportion of the integrated fluorescence power at low concentrations of quinine sulfate. With an integration time of 10 s, the detection limit for quinine sulfate is 3.0×10^{-9} M (2.3 ppb) at an S/N ratio of 3.4 ($n = 3$).[11] At high concentrations, there is no curvature or other evidence of absorbance effects because of the short pathlength of the capillary flow cell. Hence, the limit of linearity is determined solely by the shortest integration time of the CCD detector (0.01 s). At this integration time, the highest concentration that does not exceed the dynamic range of the A/D converter (2^{16}) is 3.0×10^{-4} M (230 ppm). Thus, the linear range of the calibration curves for quinine sulfate is 1.0×10^5.

The effect of quinine sulfate concentration on the S/N ratio is shown in Fig. 3B. This logarithmic graph shows two distinct regions of behavior. The first occurs at signal levels above 10^3 counts, where the slopes range from $m = 0.50–0.80$ ($r^2 = 0.993–1.000$, $n = 2–3$) and generally increase with integration time. This slope implies that the noise is proportional to the square root of the signal and that the system is exhibiting shot-noise-limited behavior, as described above. At lower signal levels, however, the S/N ratio becomes linearly dependent on the signal, with slopes ranging from $m = 0.88–1.05$ ($r^2 = 0.981–1.000$, $n = 2–3$). This slope implies that the noise is independent of the signal and that the system is exhibiting blank-noise-limited behavior. Additional studies have indicated that this noise is predominantly due to dark and read noise of the CCD, with a smaller component due to fluctuations in the background arising from laser scatter and other stray light. The dark current is largely independent of integration time up to 1 s (e.g., 1303 ± 14 counts), but increases significantly thereafter. Thus, the region with blank-noise-limited behavior appears at higher signal levels with increasing integration time in Fig. 3B.

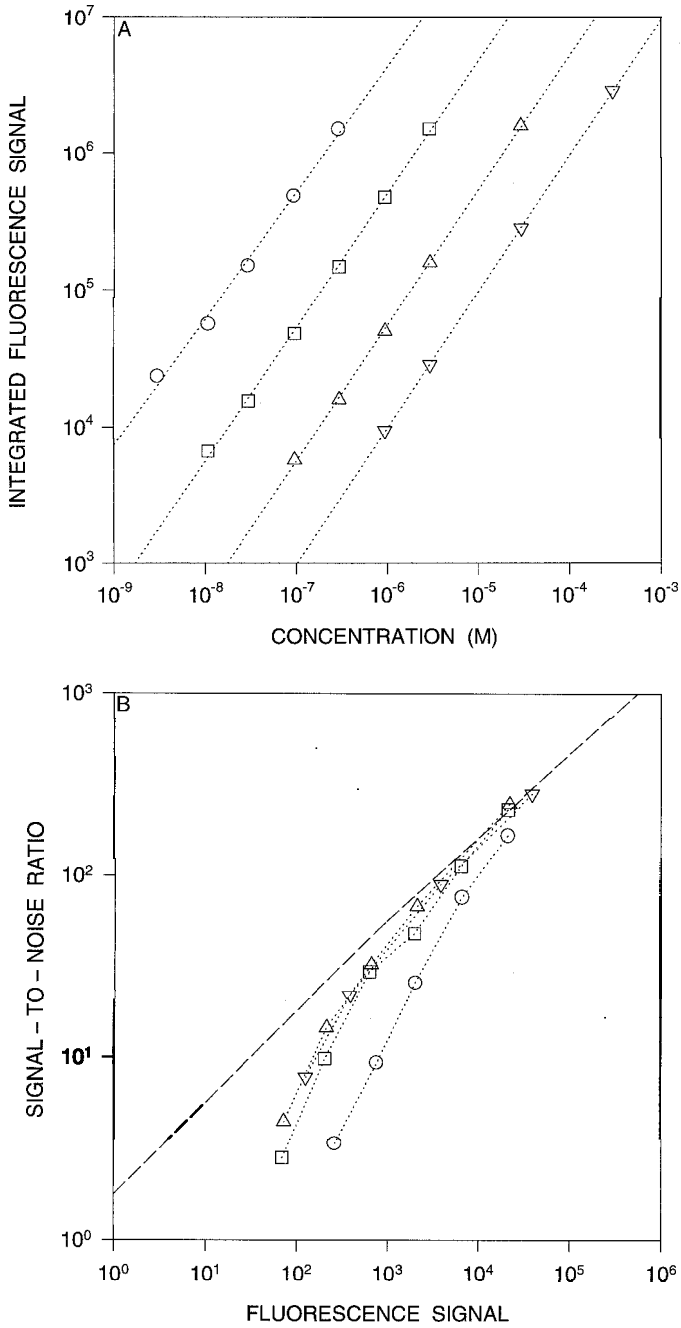

FIG. 3. Effect of quinine sulfate concentration on the signal (**A**) and S/N ratio (**B**) using integration times of 0.01 s (▽), 0.1 s (△), 1 s (□), and 10 s (○). Other experimental conditions as described in Fig. 2.

Overall, these studies have indicated that optimum performance of the system can be achieved by first reducing the background to its fundamental limit. This limit is determined by the dark and read noise of the CCD.[15] Once this has been achieved, the integration time can then be adjusted to control the signal level and maximize the S/N ratio. Ideally, the signal level should be near the upper limit of the dynamic range of the A/D converter so that the subsequent fluorescence quenching measurements will have the largest possible linear range.

Quenching Studies. The ability of the fluorescence system to measure quenching constants accurately has been assessed by using two well-known and well-characterized quenchers: nitromethane and triethylamine. Both of these compounds are effective quenchers of polycyclic aromatic hydrocarbons (PAHs), which are an important group of pollutants found at trace levels throughout the environment. PAHs form the largest known class of chemical carcinogens and mutagens and have been identified by the U.S. Environmental Protection Agency as priority pollutants.[16,17] Structurally, PAHs consist of two or more fused aromatic rings that can exist in many isomeric arrangements. These isomers are organized into two main classes; alternant PAHs have a fully conjugated aromatic system, whereas nonalternant PAHs have disrupted aromaticity due to the presence of five-membered rings.[16,17] Sawicki et al. first reported that nitromethane, an electron acceptor, selectively quenches the fluorescence of alternant PAHs compared with their nonalternant isomers.[18] Subsequent systematic studies by Acree and co-workers have shown that the so-called "nitromethane selective quenching rule" is broadly applicable with only a few exceptions.[19–23] Although triethylamine has been identified as an effective quencher of PAH fluorescence,[24,25] only one published report to date has indicated any selectivity.[26] As an electron donor, triethylamine would be expected to show selectivity for nonalternant PAHs over their alternant isomers.

Two representative pairs of PAHs have been selected for this study: pyrene and fluoranthene, as well as benzo(*a*)pyrene and benzo(*b*)fluoranthene. These isomeric PAHs have the same molecular formula, the same number of aromatic rings, and a similar length-to-breadth ratio, differing only in their alternant/nonalternant ring structure. Figures 4A and 4B show the Stern–Volmer plots for these representative PAHs with triethylamine and nitromethane, respectively, as quenchers. These plots are constructed from fluorescence power ratios derived from the integrated emission spectra, as described previously. Both quenchers are demonstrating the expected selectivity for PAH isomers, with nitromethane being a more effective quencher of the alternant PAHs and triethylamine being a more effective quencher of the nonalternant PAHs. The linearity of the Stern–Volmer plots is best for those fluorophore–quencher systems with large quenching constants, where the correlation coefficients range from $r^2 = 0.998$–1.000. Determination of smaller quenching constants is necessarily more difficult as the smaller differences in the fluorescence power ratio are more sensitive to random errors in concentration and instrumental response.[5] As a result, these quenching constants have lower correlation coefficients of $r^2 = 0.889$–0.995. The y intercepts for all plots fall within the range of 0.98–1.09, as expected from Eq. 1. Finally, there is no evidence of curvature in the Stern–Volmer plots, which would be indicative of either absorbance effects or static quenching.

Table I compares the quenching constants for the PAHs with triethylamine determined from Fig. 4A with those obtained by using a commercially available scanning fluorimeter with a 1 cm cuvette cell. The agreement is quite good and, in general, the Stern–Volmer constants determined by using the two systems are statistically indistinguishable. The small discrepancies may arise from differences in the spectral bandpass, which is 1 nm for the present system and 2.5 nm for the conventional fluo-

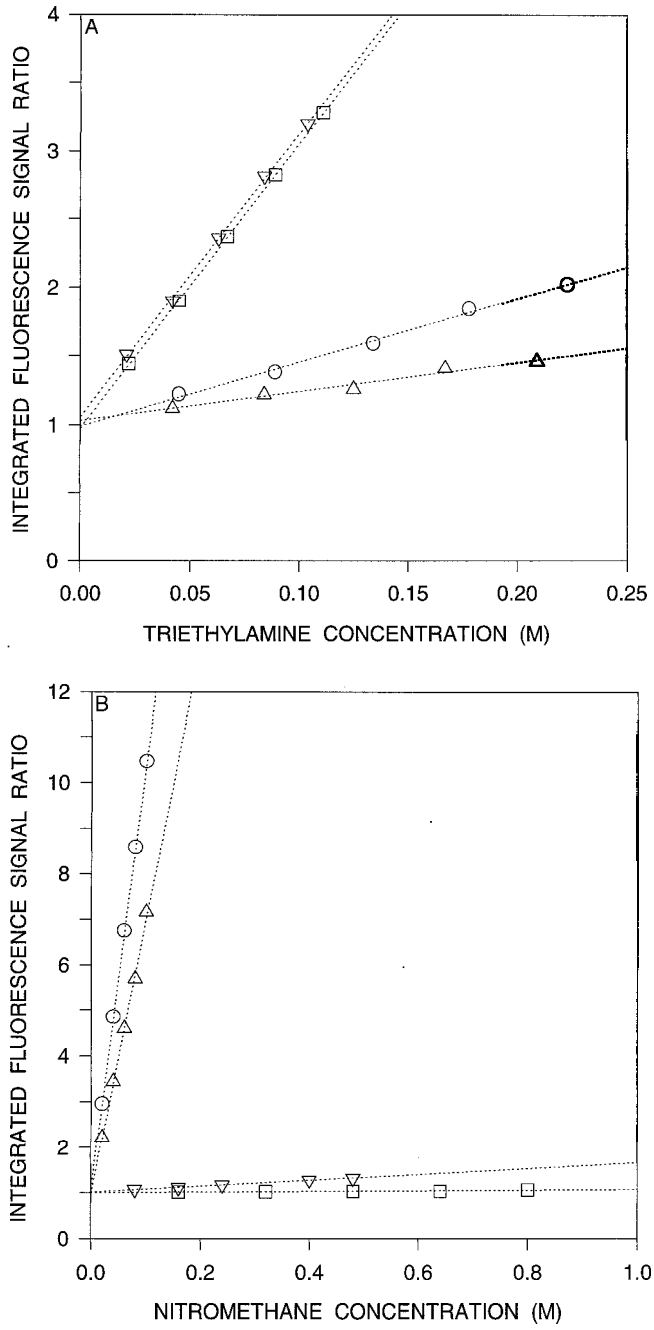

FIG. 4. Stern–Volmer plots for the quenching of 10^{-5} M pyrene (○), fluoranthene (□), benzo(*a*)pyrene (△), and benzo(*b*)fluoranthene (▽) by triethylamine (**A**) and nitromethane (**B**) in methanol. Other experimental conditions as described in Fig. 2.

rimeter. The linearity of the Stern–Volmer plots for the present system is at least comparable to and, in some cases, superior to that for the conventional fluorimeter with absorbance corrections via Eq. 3. Table II compares the quenching constants for the PAHs with nitromethane determined from Fig. 4B with previously published results.[4,5] Again, the agreement is reasonably good in spite of significant differences in instrumentation and experimental methods. Thus, the performance of the present system has been validated by comparison to traditional methods by using premixed solutions for the determination of Stern–Volmer quenching constants.

A powerful modification of this system is to use flow injection techniques[27] to automate the measurement of quenching constants, as shown in Fig. 1. This approach facilitates the rapid determination of quenching constants with minimal solution preparation, requiring only one solution of the fluorophore and one of the quencher. A dual-piston syringe pump is used to deliver the quencher solution in a step gradient, which offers several advantages over the linear gradient used in previous work.[8] Each step is programmed for a specified duration, which allows for replicate injections of a single fluorophore or injections of several fluorophores. The concentration of the quencher is accurately known and does not vary over the width of the fluorophore zone. The fluorophore zones are injected in sufficiently large volume for them to form flat-topped peaks. In this way, the concentration at the zone center is the same as that in the prepared solution and is not dependent on the broadening processes in the flow injection system. Hence, the resulting precision of the quenching constants is independent of fluctuations in flow rate, injection volume, etc. Moreover, the flat-topped profile enables the integration time of the CCD detector to be varied as necessary to achieve the optimal S/N ratio and linear range. Finally, the method of merging zones is used in order to ensure adequate mixing of the fluorophore and quencher solutions.[27]

An example of the data resulting from this flow injection approach is illustrated in Fig. 5 for pyrene quenched by nitromethane. The lower trace from the UV-visible absorbance detector at 254 nm shows the step gradient of the quencher ranging in concentration from 0 to 0.05 M in increments of 0.01 M, together with triplicate injections of the fluorophore at each step. This absorbance trace provides independent verification of the fluorophore and quencher concentrations and their precisions as well as evidence for or against static complexation. The middle trace shows the fluorescence of pyrene with excitation at 325 nm and emission detected by the PMT detector at 371 nm. The decrease in fluorescence power with increasing nitromethane concentration is evident, and pro-

TABLE I. Stern–Volmer constants for polycyclic aromatic hydrocarbons with triethylamine in methanol.[a]

PAH	Classification	K_d (M^{-1})[b]	$s(K_d)$ (M^{-1})[b]	(r^2)[b]	K_d (M^{-1})[c]	$s(K_d)$ (M^{-1})[c]	(r^2)[c]
Pyrene	Alternant	4.4	0.3	0.986	4.6	0.2	0.996
Benzo(*a*)pyrene	Alternant	1.8	0.2	0.967	2.1	0.2	0.974
Fluoranthene	Nonalternant	23.0	0.6	0.998	20.7	0.1	1.000
Benzo(*b*)fluoranthene	Nonalternant	21.7	0.3	0.999	20.6	0.4	0.999

[a] K_d = Stern–Volmer constant; $s(K_d)$ = standard deviation of Stern–Volmer constant; r^2 = square of correlation coefficient.
[b] Use of a 1 cm cuvette cell; this work.
[c] Use of a 75 μm capillary cell; this work.

TABLE II. Stern–Volmer constants for polycyclic aromatic hydrocarbons with nitromethane in methanol.[a]

PAH	Classification	K_d (M^{-1})[b]	K_d (M^{-1})[c]	(r^2)[c]	K_d (M^{-1})[d]	$s(K_d)$ (M^{-1})[d]	(r^2)[d]
Pyrene	Alternant	125	100	0.999	94	0.3	1.000
Benzo(*a*)pyrene	Alternant	—	67	0.998	61	1.6	0.998
Fluoranthene	Nonalternant	0.15	1	0.954	0.07	0.01	0.900
Benzo(*b*)fluoranthene	Nonalternant	—	2	0.994	0.64	0.02	0.997

[a] K_d = Stern–Volmer constant; $s(K_d)$ = standard deviation of Stern–Volmer constant; r^2 = square of correlation coefficient.
[b] Use of a 1 cm cuvette cell, absorbance correction via Eq. 3; Ref. 4.
[c] Use of a 1 cm cuvette cell, absorbance correction via Eq. 3; Ref. 5.
[d] Use of a 75 μm capillary cell; this work.

vides the information necessary for the determination of the Stern–Volmer quenching constant and its precision at a single wavelength. Finally, the upper traces show the fluorescence spectra of pyrene obtained with the CCD detector, which are used to determine the quenching constant and its precision at a single wavelength (371 nm) or over an integrated range of wavelengths (350–500 nm).

Table III summarizes the quenching constants determined from this flow injection experiment as well as a comparison to the static system with premixed solutions, as described above. These results confirm that quenching constants determined by flow injection are statistically equivalent to those determined by static measurements, both of which show a high degree of linearity (r^2 = 0.999–1.000). In addition, the quenching constants ob-

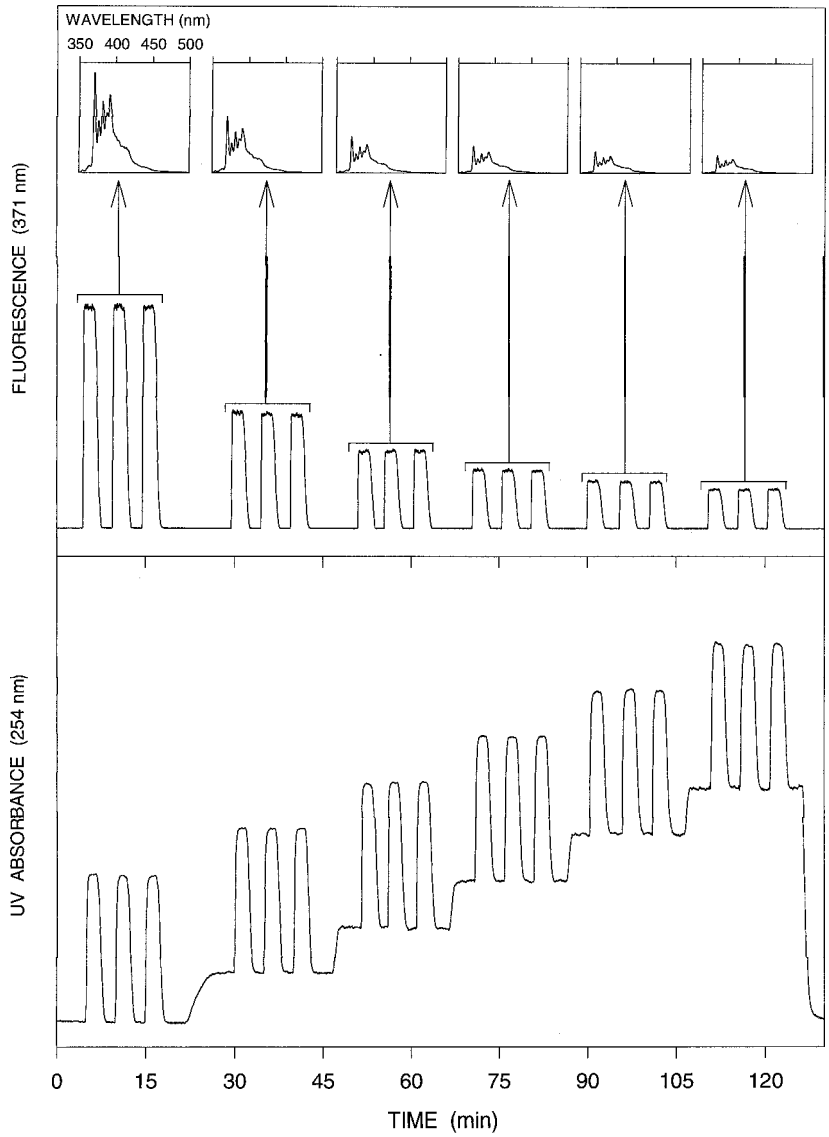

FIG. 5. Experimental data obtained by using the flow injection approach to determine Stern–Volmer constants. Fluorophore: 75 μL injections of 10^{-5} M pyrene in methanol, 35 μL/min. Quencher: 0.0–0.05 M nitromethane in increments of 0.01 M per 20 min step, 35 μL/min. Lower trace shows UV absorbance at 254 nm. Middle trace shows fluorescence detected by PMT at 371 nm, 1 nm bandpass. Upper traces show fluorescence spectra detected by CCD detector at 350–500 nm, 1 nm bandpass, 0.2 s integration time. Other experimental conditions as described in Fig. 2.

TABLE III. Comparison of experimental methods for the determination of Stern–Volmer constants for pyrene with nitromethane in methanol.[a]

Method	Detector	Wavelength (nm)	Pathlength (μm)	K_d (M^{-1})	$s(K_d)$ (M^{-1})	b	r^2	n
Static	CCD	371	75	103.0	0.99	1.02	1.000	5
Static	CCD	350–500	75	93.8	0.33	1.09	1.000	5
Flow injection	PMT	371	200	96.1	0.35	0.99	1.000	5
Flow injection	PMT	371	200	95.5	0.13	1.00	1.000	50
Flow injection	CCD	371	200	96	1.4	0.89	0.999	5
Flow injection	CCD	350–500	200	91	1.7	0.92	0.999	5
Flow injection	CCD	371	200	97	1.1	0.90	1.000	50
Flow injection	CCD	350–500	200	92	1.3	0.93	0.999	50

[a] K_d = Stern–Volmer constant; $s(K_d)$ = standard deviation of Stern–Volmer constant; b = y-intercept; r^2 = square of correlation coefficient; n = number of measurements at each quencher concentration.

tained with the PMT detector are comparable in magnitude but higher in precision than those obtained with the CCD detector at the same wavelength. When the number of measurements (n) at each quencher concentration is increased from 5 to 50, the magnitude of the resulting quenching constants remains relatively constant and the precision is improved. However, the PMT detector shows a more significant improvement in precision than the CCD detector, which is limited by dark and read noise. Finally, the quenching constants calculated at a single wavelength of 371 nm tend to be larger in magnitude than those calculated over an integrated wavelength range of 350–500 nm. This observation suggests that this vibronic transition of pyrene interacts differently with nitromethane when compared to the integrated emission spectrum. This conclusion is consistent with previous measurements of the quenching of pyrene by nitromethane at a series of single wavelengths.[5] In cases such as this, the integrated spectra can provide more reproducible and reliable quenching constants. This approach is also beneficial for fluorophores with emission spectra that are highly structured or that vary with the concentration of the quencher or solvent.[4,5]

CONCLUSION

Although selective fluorescence quenching is a promising technique, only a few fluorophore–quencher systems have been characterized in sufficient depth and detail to permit their use for routine analysis. The further development and application of this technique will require more rapid and accurate methods for the determination of Stern–Volmer constants. The system developed in the present work automates the preparation and mixing of fluorophore and quencher solutions by means of capillary flow injection methods. The small diameter of the capillary allows the fluorescence measurements to be made without interference from primary and secondary absorbance effects. The fluorescence spectrometer is equipped with a charge-coupled device that has a detection limit of 3.0×10^{-9} M (2.3 ppb) and a linear range of 10^5 with integration times of 0.01–10 s. This spectrometer has a 300 nm spectral range with 1 nm resolution, which allows the Stern–Volmer constants to be calculated at single wavelengths or over integrated wavelength ranges. This system was validated by determination of the quenching constants for selected alternant and nonalternant PAHs as fluorophores with nitromethane and triethylamine as quenchers. These quenching constants compare favorably with those determined by traditional methods in terms of both accuracy and precision.

ACKNOWLEDGMENTS

The authors gratefully acknowledge the technical support of Mr. Michael Hasselhuhn of the Melles Griot Laser Group. This research was supported by the U.S. Department of Energy, Office of Basic Energy Sciences, under Grant Number DE-FG02-89ER14056. In addition, the support of the National Science Foundation by means of a graduate research fellowship to J.V.G. is gratefully acknowledged.

1. V. L. McGuffin and J. V. Goodpaster, ''Polycyclic Aromatic Compounds, Fluorescence Quenching'', *Encyclopedia of Environmental Analysis and Remediation,* R. A. Meyers, Ed. (John Wiley and Sons, New York, 1998), pp. 3814–3831.
2. J. Lakowicz, *Principles of Fluorescence Spectroscopy* (Plenum Press, New York, 1983).
3. R. Badley, *Fluorescence Spectroscopy* (Plenum Press, New York, 1983).
4. S. H. Chen, C. E. Evans, and V. L. McGuffin, Anal. Chim. Acta **246,** 65 (1991).
5. F. K. Ogasawara, Y. Wang, and V. L. McGuffin, Appl. Spectrosc. **49,** 1 (1995).
6. C. E. Bunker, Y. Sun, and J. R. Gord, J. Phys. Chem. A **101,** 9233 (1997).
7. P. K. Behera, T. Mukherjee, and A. K. Mishra, J. Lumin. **65,** 131 (1995).
8. D. J. Desilets, P. T. Kissinger, and F. E. Lytle, Anal. Chem. **59,** 1244 (1987).
9. A. Savitsky and M. J. E. Golay, Anal. Chem. **36,** 1627 (1964).
10. X. Lu and E. S. Yeung, Appl. Spectrosc. **49,** 605 (1995).
11. J. J. Cetorelli, W. J. McCarthy, and J. D. Winefordner, J. Chem. Educ. **45,** 98 (1968).
12. C. Th. J. Alkemade, W. Snelleman, G. D. Boutilier, B. D. Pollard, J. D. Winefordner, T. L. Chester, and N. Omenetto, Spectrochim. Acta, Part B **33,** 383 (1978).
13. G. D. Boutilier, B. D. Pollard, J. D. Winefordner, T. L. Chester, and N. Omenetto, Spectrochim. Acta, Part B **33,** 401 (1978).
14. Y. P. Sun, B. Ma, G. E. Lawson, C. E. Bunker, and H. W. Rollins, Anal. Chim. Acta **319,** 379 (1996).
15. J. V. Sweedler, Crit. Rev. Anal. Chem. **24,** 59 (1993).
16. M. L. Lee, M. V. Novotny, and K. D. Bartle, *Analytical Chemistry of Polycyclic Aromatic Compounds* (Academic Press, New York, 1981).
17. T. Vo-Dinh, *Chemical Analysis of Polycyclic Aromatic Compounds* (John Wiley and Sons, New York, 1989).
18. E. Sawicki, T. W. Stanley, and W. C. Elbert, Talanta **11,** 1433 (1964).
19. W. E. Acree, Jr., S. Pandey, S. A. Tucker, and J. C. Fetzer, Polycyclic Aromat. Compd. **12,** 71 (1997).
20. S. A. Tucker, H. C. Bates, V. L. Amszi, W. E. Acree, Jr., H. Lee, P. Di Raddo, R. G. Harvey, J. C. Fetzer, and G. Dyker, Anal. Chim. Acta **278,** 269 (1993).
21. S. A. Tucker, J. M. Griffin, W. E. Acree, Jr., P. J. Mulder, J. Lug-

tenburg, and J. Cornelisse, Analyst **119,** 2129 (1994).
22. S. A. Tucker, H. C. Bates, W. E. Acree, Jr., and J. C. Fetzer, Appl. Spectrosc. **47,** 1775 (1993).
23. S. A. Tucker, J. M. Griffin, W. E. Acree, Jr., J. C. Fetzer, M. Zander, O. Reiser, A. De Meijere, and I. Murata, Polycyclic Aromat. Compd. **4,** 141 (1994).
24. J. Mai, J. Cheng, and T. Ho, J. Photochem. Photobiol. A **66,** 53 (1992).
25. M. Vasilescu, Rev. Roum. Chim. **34,** 1819 (1989).
26. M. P. Fogarty and I. M. Warner, Appl. Spectrosc. **36,** 460 (1982).
27. J. Ruzicka and E. H. Hansen, *Flow Injection Analysis* (John Wiley and Sons, New York, 1988).